Additively manufactured three dimensional reference porous media for the calibration of permeability measurement set-ups

M. Bodaghi, D. Ban, M. Mobin, C.H. Park, S.V. Lomov, M. Nikzad

Additively Manufactured Three Dimensional Reference Porous Media for the Calibration of Permeability Measurement Set-ups

M. Bodaghi[a,b], D.Ban[c], M.Mobin[c], C.H.Park[a,b] , S.V.Lomov[d], M.Nikzad[c]*

[a] IMT Lille Douai, Institut Mines-Télécom, F-59508, Douai, France

[b]Université de Lille, F-59000, Lille, France

[c] Faculty of Science, Engineering and Technology, Swinburne University of Technology, Hawthorn, Victoria Australia 3122

[d] Department of Materials Engineering, KU Leuven, Leuven, Belgium

[*] Corresponding author:

E-mail: masoud.bodaghi@imt-lille-douai.fr

Tel: (+351) 0327712330

Abstract

This paper presents the first comparative study of fabricating reference porous media with three different additive manufacturing (AM) techniques, namely Fused Deposition Modelling (FDM), Stereolithography (SLA) and HP Multi Jet Fusion (MJF). Various parameters in each step of these 3D printed reference media that contribute to model inaccuracy, including the intrinsic limitations of each printing technology are examined. The analysis of repeatability and dimensional accuracy of 3D printed parts shows that SLA yields the highest integrity in 3D printed reference medium with tolerances well below 2% of the nominal thickness of the mould. Hence the reference medium processed via SLA is tested for the permeability study. Statistical analysis based on 20 measurements of permeability using the same set-up shows a coefficient of variation of less than 2%, confirming the elimination of the inherent source of variability in real textile.

Keywords: E. 3-D Printing; B.Permeability; E.Porosity; C.Statistical Analysis

1. Introduction

The goal in liquid composite moulding (LCM) process is filling all the empty spaces (channels) between and within fibre tows with resin in a reliable way and complete it in the shortest time possible. Permeability which is defined as the ease of flow through a textile preform can substantially influence quality of parts produced by LCM [1]. Permeability is a function of reinforcing textile's architecture and porosity. A typical textile reinforcement has two dimensions of channels which form dual-scale porosities. The width of channels between tows can range from 80 µm to 250 µm (Fig.1-a) and the fibres with the scale of 7 µm can form channels with the dimension of about 1 µm (Fig.1-b), and together they create a tow [2]. Intra-tow porosity is formed by the channels between fibres and

inter-tow porosity is formed by the channels between tows. Such a dual-scale porosity in a textile preform creates differential permeabilities of high (inter-tow) and low (intratow) zones [3]. Therefore, the flow through the heterogeneous medium forms fingering or saturation lead-lag flow due to the imbalance of flow rate between intra-tow and inter-tow zones, which can create manufacturing defects such as voids and dry spots [4,5].

Fig. 1: The schematics of the dual porosity: (a) a 2/2twill woven carbon composite cross section, orthogonal to the warp (channels between tows forming inter-tow porosity), (b) Fibres inside a tow (channels between the fibres forming intra-tow porosity) the images with permission from [6].

The important role of permeability in the field of flow modelling and composite manufacturing has led researchers to spend decades working to develop effective experimental and modelling approaches and methodologies that establish reliable methods for permeability measurement and prediction. Since there is no standard method of measurement of textile preform permeability, researchers and different laboratories around the world were required to develop their in-house permeability measurements instruments. This often resulted in contradictory data of permeability values determined by laboratories with the in-house set-ups. This has led to a number of permeability benchmark exercises worldwide [7–9]. However, even with the results of these permeability benchmarks, some issues remain regarding the understanding of the fundamentals of the variability and uncertainty behind the experimental permeability measurement instruments. A major problem in comparing different permeability test methods has always been the fact that there exists no reliable reference template against which a comparative permeability measurement can be performed [10]. A reliable reference porous medium is needed not only to calibrate a permeability measurement set-up but also to compare different permeability measurements and validate the numerical permeability computation software. Unlike real textile preform, the permeability of such a reference porous medium is consistent at different measurement runs or does not vary widely from test to test. Hence, a reference medium helps in understanding the sources of uncertainty related to the test rig.

In dealing with any discrepancy between different measurement instruments, Parnas and Salem [11] suggested the use of a 3D woven fabric mat as a reference porous medium. A coefficient of variation of 15% was obtained for the measured permeability values of the standard reference medium in different runs. In another attempt, Parnas [12] analysed permeability database of fibres mats provided by the National Institute of Standards and Technology. They observed a coefficient of variation of 20% for the woven, unidirectional and stitched mats and more than 50% for random mats. However, as the absolute permeability of these various mats was unknown, the accuracy of these permeability measurements remained unknown. In addition, the usefulness of such reference materials might be reduced by the permeability variations of these reference fibre-mats due to race tracking and/

or the inherent variation of mat porosity. Lundstrom [13] made the permeability reference by a number of capillary tubes in one of the four-cavity permeability measuring set-up. But it is to be noted that the accuracy of the three main cavities for the measurement of the preform permeability in three different directions (0º, 45º, and 90) was not guaranteed through the device. To calibrate rectilinear flow mould, Roy [14] used a reference medium consisting of a row of parallel holes in the flow direction. Later, Tan and Pillai [15] used a reference medium consisting of two concentric annular slits for the calibration of their radial flow mould. In both of these cases, as the flow rate increases, the difference between the experimentally measured permeability and the numerically-estimated permeability increases due to mould deflection. The disadvantages are that the reference media share high coefficient of variations during the permeability measurements. Hence, the first challenge for such a reference platform is to manufacture a porous medium with controlled porosities. 3D printing (3DP) techniques, a.k.a. "AM" or "rapid prototyping", offer the potential to fabricate the porous medium with controlled porosity [16]. Morren *et al.* [10] manufactured a three-dimensional reference medium with lattice-like microstructure from liquid photosensitive polymers using stereolithography. Using this reference medium, a coefficient of variation of 5% was reached for the radial flow mould. However, little information was provided in terms of the quality of the printed templates, repeatability, dimensional and geometrical accuracy, and surface texture, which are crucial data for establishing elements such as dimensional and geometrical tolerances, surface finish, and correct printer set-up and functioning, and the manufacture of prototypes. Although, the work done by Morren *et al.* [10] has been a pioneer in the application of 3DP technology for the manufacturing scalable textile-like porous models, there is a need for further research exploring various 3D printing teachnlogies and the fundamental mechanisms of fabrication they employ as well as the effect of printing materials on the quality and reliability of printed refrence medium For example, the repot by Morren *et al.* [10]did not address how different 3DP techniques and materials can replicate pore networks of a textile preform. In addition, their geometry had uniform porous structures. , In the the current study? the proposed geometry model therefore features some degree of complexity by adding anisotropic porous structure in x and y directions. This anisotropy is relevant not only in testing the efficacy of the 3D printing teahcinques for fabricating reliable refrence porous media but also for the calibration of a central injection system.

2. Previous Work on precision of 3D printing

3DP is a generic term for techniques by which solid objects are fabricated from Computer-aided Design (CAD) models in a layer-by-layer fashion. In 1984, Charles Hull patented the first working 3D printer known as Stereolithography (SLA) to fabricate complex 3D geometry plastic parts. Since then, subsequent 3DP systems,

including Powder Bed Fusion (PBF), e.g. Selective Laser Sintering (SLS) and Multi Jet Fusion (MJF), Material Extrusion, e.g. Fused Deposition Modelling (FDM), and Material Jetting (MJ) have been developed. Several recent papers [17–20] have reviewed the developments and advances in 3DP techniques and corresponding materials.

The use of AM has risen in the leading industry sectors such as aerospace, automotive and healthcare over the last decade mainly due to the need to reduce the time to market and build functional prototypes at the lowest cost. The capabilities to build consolidated components irrespective of geometryical complexities gave the ability to designers to create products without the need for dedicated tools and forms not otherwise achieveable by conventional techniques. This brought great freedom to the designer and an economic advantage [21–23].

Recently, 3DP has allowed for the fabrication of porous media in the forms of lattices, cellular structures, and foams. The potential uses of 3DP within the porous media structures are vast, with applications ranging from 3D printed granular media from real sand grains for geotechnical testing [24] to the 3D printed ordered porous media as a reference sample for comparison of permeability results from different test set-ups [10]. For the 3D printed porous media with controlled porosity, including pore shape and size distribution, understanding of dimensional accuracy is vital. For example, the medial distribution in the pore size should be limited to 2% of the total thickness of the porous medium for the calibration of the permeability measurement set-up. The 2% limit was proposed for the deviation of the cavity thickness on the guideline for Benchmark II [25]. While the given limit to the deviation of thickness does not completely reflect the mould deflection during the permeability experiments, this deviation provides a quantified estimate of the uncertainty from target cavity thickness. This makes it essential that the dimensional accuracy of the 3D printed part is kept at the required level. Hence, it necessitates a thorough study to investigate the expected dimensional accuracy of the parts fabricated by 3DP.

Previous studies have mainly focused on the dimensional stability of the final part and the relationship between process parameters and post-curing accuracy. For the FDM, Masood [26] minimized the volumetric error in the 3D printed part by a generic part orientation optimization. Wang [27] numerically analysed the influence of the process parameters, i.e. slice numbers, stacking section length, chamber temperature, and material linear shrinkage, on the warp deformation of 3D printed part. Sood [28] experimentally investigated the influence of process parameters, i.e. layer thickness, part orientation, raster angle, air gap and raster width along with their interactions on the dimensional accuracy of FDM part. In a recent study, Dixit [29] studied the contribution of processing parameters, i.e. raster width, slice height, and path speed of FDM to the dimensional accuracy of 3D open-source product. In another study on the total dimensional error of a representative part fabricated by FDM,

the effects of four process parameters, i.e. infill shape, infill density, the number of perimeters created per layer, and layer height were analysed [30]. For the SLA, Lee [31] predicted the effects of the process parameters, i.e. the layer thickness, fill spacing, fill cure depth, hatch overcure, and hatch spacing, on the dimensional accuracy of printed parts by a neural network approach. Huang and Lan [32] simulated the SLA process by applying dynamic finite element method and reduced the dimensional error of final parts through reverse compensation. Jayanthi [33] performed an Analysis of Variance (ANOVA) to study the effects of process parameters, i.e. layer thickness, writing style, hatch spacing, hatch overcure and fill cure depth, on the curl distortion of the final parts printed by SLA. For the PBF, Senthilkumaran [34] investigated the effect of SLS process parameters, i.e. exposure strategies, build orientation, etc, on the shrinkage behaviour of the Polyamide 12 (PA 12) samples with different sizes. Shi [35] designed a benchmark specimen and examined the dimensional accuracy of the as-printed SLS polystyrene sample and the sample which was infiltrated with epoxy resin. The results showed that both as-printed and post-processed samples had a good accuracy, less than 2% of the designed size. Singh [36] developed mathematical models representing the relation between the process parameters and the dimensional accuracy of the SLS printed PA parts. Then, the optimal levels of the parameters were found through optimization approaches, i.e. Response Surface Methodology (RSM) and Desirability Function (DF). Their results showed that the dimensional accuracy of SLS PA parts increased with the increase in laser power and bed temperature, while it decreased by increasing scan spacing.

It follows from the preceding discussion that the influence of process parameters on the dimensional accuracy of the 3DP machine has been analysed. The understanding of material shrinkage and curling phenomena has been well documented in the literature. However, little has been done to investigate the consistency and repeatability of different aspects of the part fabricated by 3DP relevant to permeability measuremnets for applications such as LCM. It is extremely difficult to design a universal test part for process optimization due to the great variety of working principles at the base of AM technologies. According to Cho [38,39], very little literature about the AM of scale models existed. Most of those studies, based on dimensional analysis, only experimentally analysed the test results without providing a way to improve the accuracy of those test results [40]. No prior studies have examined how different 3DP techniques can replicate pore networks simply, rapidly, and accurately.

The porous structures have been synthetically produced by liquid-state processing, solid-state processing, electrodeposition and vapour deposition [22]. However, only limited control over the internal structure can be achieved by these processes. Although the shape and size of the pores can be adjusted by changing the parameters of these manufacturing processes, only a randomly organized porous structure can be achieved [23]. For the first

time, Fee [41] applied SLA technique to precisely replicate the fine structure of CAD models of porous media consisting of ordered particle packing and monoliths with internal channels. However, their medium did not have fixed required porosity to assure a certain permeability value, which is desirable for calibration of permeability measurement set-ups.

Despite the rapid growth of AM applications in fabrication of complex 3D porous media, the accuracy and repeatability of 3D printed models with controlled porosity and pore size have not been thoroughly investigated. Although available AM methodologies enable 3D models to be created, it is still a challenging task to print a porous medium with specific porosity and pore size value within the limits of spatial resolutions.

3. Objectives

For the accurate permeability measurement, the benchmarck I worldwide excercise [7] suggested the formulation of a guideline to be implemented in the benchmark II worldwide exercise [8]. In the benchmark II exercise [8], twelve participants followed a guideline document [25] in order to introduce better control on the experiment conditions, observed in the the first worldwide permeability benchmark [7]. The benchmark II [8] showed a much smaller variation in permeability data compared to the first data set, supporting the concepts contained in the guideline document in this second case. However, the benchmark II [8] strongly suggested that difference between experimental set-ups might be responsible for the permeability scatter due to errors on the measurement of injection pressure, fluid viscosity values, cavity height variations, race tracking and the measurement of fluid velocity. The benchmark III worldwide excersie [9] showed the largest contribution of cavity height variations to the variation between the permeability results of 19 participants, resulting in varying average coefficient of variation (c_v) between 32.2% and 43.9% for the non-crimp fabric (NCF) and woven fabric (WF), respectively, while a deviation from target cavity height smaller than 2% reduced average c_v to 23% and 34% for NCF and WF, respectively. Hence, the appropriate design of experimental set-ups can strongly reduce the influence of the cavity height variation.

The target of the benchmarking efforts is to reach a point at which the variation between the results gained with different measurement set-ups is no larger than the variation between results gained on a single system [9]. This leads to requirements for the repeatability of the permeability measurements and tolerances for the mould geometry [8,9,25]. As the permeability cannot be characterised by a single value [42], the authors believe that multiple samples with these requirements can provide the desired permeability measuremnets from test to test. These requirements are summarised in Table 1. based on guidelines and “boundary conditions” for the development of the 3DP reference medium for the permeability measurements. This 3DP reference medium

resembles a typical reinforcement and avoids the sources of permeability scatter including nesting, shearing and compression of the textile layers, mixture of low and high permeability zones, and saturated and non-saturated fluid flow. As stated earlier, the dual-porosity nature of a textile preform leads to intra- and inter-tow values for permeability. Belov *et al.* [43], Wang [44] and Nabovati [45], reported the difference of 10 to 30% in the computed global permeability of woven textiles for the cases of permeable and impermeable tows. This difference justifies the model which considers solid tows is reasonable because standard devations of 20-30% are common for the experimental results. Consequently, the current study focuses on inter-tow porosity which is the main factor defining permeability of woven, braided and knitted textile reinforcement [46]. The authors are aware that intra-tow permeability has an increasing contribution to global permeability as the global fibre volume fraction increases. However, the geometry with solid tow allows the excellent repeatability of permeability experiments from test to test.

Table 1: The requirements of the production of a 3DP reference

Such a reference porous medium can be used for the calibration of permeability measurement set-ups and for the comparison of permeability results from different measurement set-ups. The reference medium also allows a correct and full definition of the geometry in the numerical permeability computation software due to a simple unit cell. To that end, it is necessary to select an appropriate AM technique through a robust dimensional accuracy analysis of reference samples printed via aforementioned technologies. This work provides much detail on how different manufacturing strategies would accomplish this goal. Thus, ultimately, the aim of this study is to assess the quality parameters for the manufacture of textile-like porous medium using FDM, SLA, and HP MJF as the leading commercial mid-range 3D printering format from a geometric perspective to determine dimensional precision, flatness error, and the characterization of surface texture (Fig.2). This data is vital for determining the quality of the final product and provides users with essential information on the tolerance of these three AM technologies for fabricating the select porous reference media for future permeability benchmarking exercises.

It is worth emphasizing that we are aware that the direct comparison about accuracy and precision among all available 3DP technologies is not entirely possible. With the use of available 3DP technologies and carefully validated workflows, one or more of steps involved in 3DP is carried out with limited accuracy and repeatability due to inappropriate use of or over-reliance on the underlying technologies. As more evidence gathers by the literature and the use of 3DP becomes more common, manufacturers will need to be able to report their techniques and validate them by using appropriate accuracy. This is a complex task, with no single variable being

representative of the comprehensive 3D printed models for all indications. The metrics of 3D printed model accuracy described in this article are critical to establish and substantiate appropriate textile-like porous medium for permeability benchmark practice. The ultimate goal is to enable the development of guidelines for the manufacturing of textile-like reference medium for the calibration of permeability set-ups. For those involved in permeability benchmark practices, these metrics can be used to validate new and optimised textile-like reference medium model that facilitate the faster, more accurate and reproducible 3D printed reference medium.

Fig. 2: Integrated flow diagram for the selection of 3DP technique for manufacturing tangible textile-like porous medium

2. Experimental details

Within this study, three leading 3DP methods, namely SLA, MJF, and FDM have been used to develop competitive and flexible routes for the fabrication of textile-like porous medium with the highest dimensional accuracy.

2.1 Design and fabrication of the porous medium

As part of the development of a guidline for the calibration of permeability set ups and making a comparative study of different 3DP technologies, a relevant geometry demonstrator was degined, consisting of a porous medium which has the features characteristic for woven textile reinforcements in composites, namely the pore regularity, variable pore size, pore tortuosity and indirect channels without the presence of closed pores. This geometry provides a real application with a degree of complexity comparable to a typical considered woven textile and allows thisstudy to explore the effect of geometry.

The design of the textile-like porous medium is depicted in Fig.3. The porous medium was designed using ‘PTC Creo Parametric’; a CAD software package (Fig.3-a). The model (Fig.3-a) assumed solid tows (impermeable tows) for the estimation of permeability components (K_x and K_y).

The 3D representation of the pore network was created from an array of rectangular channels with two differen sizes (Fig.3-b). The CAD design was converted to tessellated format (STL- Standard Tessellation Language) which was then printed by 3D printers. The authors encourage collaboration with the interested parties in the use of the developed reference media, for example, in the scope of the International permeability Benchmark; the STL design of the reference media will be made available for partners in such collaborations.

The dimensions of the walls and the pores correspond to typical dimensions of yarns and pores in 2D and 3D textile reinforcements (see, for example [6,47,48]). Although a defined radius for the edges may resemble a real

geometry of tow, sharp edges were considered to add more complexity and better test the inherent repeatibilty issues relevant to the three 3DPs used in this study.

Fig. 3: The schematic of the textile-like porous medium: (a) A CAD geometry of the textile-like porous medium (top). (b) The dimension of the textile-like porous medium (below)

2.2 3DP machines and materials

2.2.1 SLA

SLA, the first developed and patented AM process, is categorized under Vat Photopolymerization (VP) processes according to ISO/ ASTM 52900 standard. In SLA, liquid photosensitive resin in a vat is selectively cured by light-activated polymerization. An ultraviolet (UV) laser controlled by XY scanning mirrors on galvanometers scans and exposes a light beam to the surface of liquid resin in a vat, subsequently solidifying and curing the specific areas of resin in a point-by-point style according to the cross-section of each layer.

2.2.2 FDM

In FDM, a classification of Material Extrusion (ME) processes, filament-based feedstock is selectively dispensed through a heated nozzle. FDM machine forces semi-liquid material through a nozzle as the extrusion head or the build platform moves in the XY plane. After a layer is completed, the build platform moves down, or the extrusion head moves up, and the next layer is extruded, which bonds to the previous layer. The raw material is typically a filament of thermoplastic coiled onto a spool that is melted as it is extruded. Support structures are required for overhanging features. These structures are removed, often manually, after the parts are completely built and removed from the build platform.

2.2.3 MJF

The state of the art technology, MJF is a category of PBF in which thermal energy selectively fuses regions of a powder bed. The thermal energy melts the powder material, which changes to solid phase as it cools. In MJF, semi-crystalline particulates of thermoplastic pre-polymers are used primarily as the structural material. A layer of predominantly Polyamide (PA) powder is deposited onto a build platform. Then, a print head composed of an array of nozzle jets, selectively delivers a proprietary fusing agent into the powder bed. The fusing agent is a black ink containing infrared absorbing colourants. In addition, a detailing agent is ejected into the powder bed, surrounding the edges (contours) of the part to promote resolution. The detailing agent is required to ensure the printing of sharp edges through preventing heat bleeding in the way that it creates a clear temperature difference between the build areas and unused powder surrounding it.

The polymer is heated by passing planar infrared lamps above the powder bed. The energy from the IR source is absorbed by the fusing agent and is converted to thermal energy, which successively sinters and fuses the powder bed. The process is repeated layer by layer, forming the 3D part. Moreover, glass bead blasting is used to remove the partially melted and unmelted powders from the parts. The MJF is the fastest technology commercially available to fabricate polymeric parts as opposed to other 3DP technologies, and it does not need support structures for overhanging features during layered construction.

2.2.4 Comparison of 3DP machines' specifications

In Table 2, the specifications of the 3D printer machines used in this study such as nominal lateral and Z-direction resolution and dimensional accuracy are listed. As a matter of fact, the nominal resolution and accuracy gathered in the machines' catalogues do not support the achievement of the features with this resolution and accuracy values. As a tangible example, in the laser-based technique, e.g. SLA, in addition to the laser spot size and intensity, other factors like optical properties of the resin and its parabolic curing profile, build parameters, e.g. build orientation and hatch style, and process-oriented effects, e.g. print-through effect may vary the resolution and accuracy of the parts. As nother case in point, the resolution mentioned in the FDM machines' catalogues mostly relies onthe nozzle diameter and the resolution of the stepper motors which move the carriage of the heated orifice, while the swelling rate of the filament is the most dominant factor influencing the dimensional and geometrical accuracy. Also, the lateral resolution provided by HP could be misleading as it may relate to the diameter of jet nozzles (1200 DPI or 21.17 microns) while other factors such as the particle size distribution of the powders (D90=), the surface tensions between the powders and fusing and detailing agents, which determine the sinking width and depth of the agents into the powder bed, build orientation, heat bleeding and filleting effect all influence to a degree the resolution and dimensional accuracy of the parts. In fact, these factors do not allow achieving such a small resolution of 21.17 microns and dimensional and form accuracy may vary in different conditions. For these reasons, it is required to experimentally investigate the resolution, dimensional and form accuracy and repeatability of the target 3D printers which this study covers a part of. This paper addresses two key contributing parameters to the accuracy of printed specimens including design and materials. The dimensional accuracy may vary during cooling and curing process, leading to warping or shrinkage as the specimen sizes become larger. We plan to address this problem in future work with some design recommendations. The dimensional accuracy is also influenced by materials: the accuracy of a specimen may have to sacrifice to improve some material properties.

As stated in the introduction section, it is extremely difficult to define universal processing parameters for each 3DP technologies due to the great variety of working principles at the base of AM technologies. We believe that regardless of 3DP technologies the metrics involving comparisons of specimen dimensions and morphology should be developed to quantify differences between different 3DP technologies.

Table 2: Specifications of the used 3D printer machines

2.3 Dimensional accuracy measurement

The dimensional accuracy of 3D printed porous media, the degree of agreement between the manufactured dimension and their designed specifications, is the most relevant parameter for ensuring the dimensional repeatability of manufactured parts. This study investigates the dimensional accuracy characteristics of textile-like porous media model manufactured with three different 3DP processes.

According to ASME Y14.5, the dimensional accuracy of a component part is evaluated through its size tolerance and geometric tolerance including shape, orientation, and location. Size variations in the current study were addressed by the dimension of five channel wall and pore features as shown in Fig.4. Size variation is important for defining the characteristics of a porous medium as pore size substantially influences the permeability.

The dimensional accuracy of the 3D-printed porous structures is assessed by using the Olympus BX61 Light Optical Microscope (LOM) with the dark-field illumination mode. The LOM, equipped with the digital camera and image analysis software, provides the tool for quantitative measurements. The measurements are carried out for five random locations for each feature on 3D printed samples and in five directions along with length and width of each feature (25 readings for each dimension). Then, the measurement results are compared to their designed specifications. Subsequently, the statistical significance of manufacturing techniques on the dimensional accuracy of different feature pores is examined by one-way or single-factor ANOVA.

If P-value of ANOVA analysis is less than 5%, there is a significant probability of the differences between the dimensional accuracy of different manufacturing techniques. This means that at least the measured average dimension of one of the manufacturing techniques statistically significantly varies from another manufacturing technique. However, ANOVA is an omnibus statistic test which is not able to exactly recognize where the difference between different manufacturing techniques comes from. Therefore, a Tukey HSD post hoc test, as a reliable multiple pairwise comparison test, is applied to find out the dimensional accuracy of these manufacturing techniques relevant to one another. Tukey HSD test compares each possible pair of these AM techniques.

Fig. 4: Photographs indicating dimensions of the textile-like porous medium (a) channel wall and pore features with design specification for assessment of dimensional accuracy of different 3DP techniques, (b) Five random locations used for measurement of the selected features.

2.4 Permeability measurement

The reference medium (83×93 mm^2) was placed on the steel block (800×270×40 mm^3) and within metallic spacers. The cavity height was fixed using the spacers, which was equal to the thickness of the reference medium, 5.6 mm. The top mould (PMMA) was transparent to observe the fluid flowing through the reference porous medium. A silicon rubber sealed the side walls of the mould cavity to prevent potential leaks, and minimize race tracking. This was confirmed by visual observation of impregnation process through the transparent top mould. Some race-tracking was still observable, but as the gap size was less than 0.5 mm, theinfluence of the gap on the flow front pattern was negligible (as shown in Fig.5). To reduce the risk of mould deflection, the PMMA block was reinforced with four 50 mm thick steel supports and subsequently closed with eight bolts. The sample was placed 100 mm in front of the inlet to provide uniform liquid pressure on the sample boundary. The pressure difference was measured by two pressure transducers with a distance of 450mm, located in the mould at the injected edge of the reference medium and close to the outlet.

A motor oil which closely mimics the viscous resin was used. To reduce uncertainty in permeability calculation, the viscosity(μ) of the given fluid was measured by a BROOKFIELD DV1 viscometer before and after the injection at the test temperature. The constant injection pressure directs the the Newtonian fluid unidirectionally from the injection gate on the one side of the reference medium to the outlet on the other side of the reference medium. After the saturation of the porous medium, two pressure transducers located close to inlet and outlet recorded the pressure differences between inlet and outlet. Due to two different pore sizes, Fig.5 shows the formation of fingering effect, which is an important contributor to the occurrence of bubble formation because the leading flow front can entrap air by overpassing the lagging flow front. Some of formed bubbles are transported while some of them are stationary being entrapped within channels between the solid tows during impregnation process. Bubble transportation between the tow channels is key to the unsaturated flow behaviour. This non-uniform bubble distribution can significantly influence the local pressure gradient [5]. Therefore, prior to saturated permeability measurements, the oil bleed was carried out to flush out all bubbles from the system to eliminate the sensitivity of saturated permeability results to the presence of the bubbles. Prospectively, with the precise geometry of the printed specimen associated with the isolation of the variability due to geometrical factors, the reference medium can be used to study the dependency of bubble mobility on the applied pressure or flow rate.

Fig.5: The flow front pattern during the impregnation process

The mass flow rate was calculated by recoding the mass of resin versus time at outlet. With the densities of oil (850, 860, and 880 kg/m^3), the volumetric flow rate (Q) was calculated. Subsequently, with the known pressure difference (Δp) over a distance L, and Q ,the one-dimensional version of Darcy's law yields the in-plane permeability components (Eq.1).

$$\frac{Q}{A} = -\frac{K}{\mu}\frac{\Delta p}{L} \tag{1}$$

where A is the cross-sectional area of the porous medium, and k is permeability.

3. Results

Though a single speciemen is reported for measuremnets of acuuracy and repeatability, it was not that only one single sample was printed using each teachnique here. Rather, a preliminary trial was conducted to filter out those specimens with visual defects and apparent issues around shrinkage, dimensional stabilities or any other anmolies encountered from a number of intials printes. Despite this, the claims of accuracy and repeatablities here are validated by not only conducting statistically significant number (25 across each dimesnion) of measuremnets for each of the 3D printed samles but also by examining various feature sizes, referred to here as pore (fine size) and channel wall (course) features.

3.1 Assessment of dimensional accuracy

The textile-like porous medium as a reference sample was produced with three different 3DP techniques: FDM, SLA, and MJF.

Table Table 3 summarizes the measurement results of the features selected for the assessment of the dimensional accuracy of samples. The results show that SLA sample is in much closer geometric agreement with the design and SLA technique provides the highest geometric accuracy compared to FDM and MJF.

Table 3: Measurement results of specified features for assessment of dimensional accuracy of AM techniques

The results of ANOVA confirmed that manufacturing technique has significant effect on the dimensional accuracy of specified features of reference medium. As shown in Table 4, P-value is less than 0.05 for all of the features which means that the average measured dimensions of individual features vary at least from one manufacturing technique to another one and subsequently, there are at least two manufacturing techniques whose dimensional accuracies are statistically significantly different from each other.

Conducting post hoc comparisons, using the Tukey HSD test, indicates where significant difference or similarity between the dimensional accuracy of samples printed with these three AM techniques come from. The results for the feature with length of 9.2 mm located in XY plane show that there is minor difference between the

measurement results of FDM and MJF samples (P-value= 0.609 > 0.05). Moreover, the results for the width of this feature (2 mm width) indicate that the geometric difference between SLA and MJF is small (P-value= 0.661 > 0.05) and they are in close agreement with the dimensions specified in the design, while the mean dimensions for SLA and MJF were significantly different from FDM (P-value SLA-FDM= 5.405E-008 < 0.05 and P-value SLA-MJF= 6.338E-009 < 0.05). On the contrary, the results for feature with design specification of 1.8×1.6 mm^2 located in the edge (Z direction) show that there is a significant difference in geometric results between SLA and MJF samples (P-value= 5.101E-009 < 0.05). However, for this feature there is a similarity between the measurement results of SLA and FDM samples (P-values= 0.940 and 0.055 > 0.05).

Table 4: Results of single-factor ANOVA and multiple pairwise comparison tests

Based on the measurement results shown in Fig.6 and Fig.7, the SLA specimen geometrically yielded a specimen with an accuracy close to that of specified in the design. The percentage of deviation from nominal length and width calculated for different 3DP techniques indicates that the deviation for all the measured features fabricated by SLA method falls in the range of less than 2% of the total designed dimension, while it rises up to 25% for FDM and MJF techniques, particularly for the features with nominal size less than 2 mm. Likewise, the standard deviation of the conducted meausrements for all the features printed by SLA technique has the lowest values compared to other techniques which means that SLA technique produces features with the dimensions close to the designed specification and similar dimentional values. Therefore, based on the results it can be concluded that SLA technique allows a correct import of the geometry into numerical flow simulation software (such as FlowTex [47]) for the numerical prediction of the permeability.

Fig. 6: Average measured length (a) and width (b) and percentage of deviation from nominal (c) length and (d) width of wall features with different design ratio of length to width fabricated by different 3DP techniques

Fig. 7: Average measured length (a) and width (b) and percentage of deviation from nominal (c) length and (d) width of pore features with different design ratio of length to width fabricated by different 3DP techniques.

Moreover, the measurement of the small and the large rectangle pores on the edge sides (located in the Z direction) shows that the sample printed using the FDM technique yielded a closer agreement to the design geometry in comparison with the sample printed by the MJF method. However, in terms of dimensional accuracy, the results indicate that the performance of the MJF technique to fabricate cavities in the XY plane and with the size larger than 2 mm is better than FDM technique.

3.2 Assessment of the in-plane permeability

3.2.1 Permeability measurement

As shown in the previous section, SLA manufactured the reference medium with the highest resolution and geometrical accuracy. SLA technique also resulted in the smooth surface finish which helps to avoid race tracking zone in contact with mould surface. The SLA specimen, which is designed for the rectilinear permeability measurement, consists of 9 adjacent unit cells (Fig.5). The reference medium has two dimensions of the rectangular channels, measuring 0.76 mm (width) ×2.6 mm (height) in the *Y* direction and 2.06 mm (width) ×2.6 mm (height) in the *X* direction (Fig.8). The reference medium was with some degree of complexity by adding anisotropic pore structure in *X* and *Y* directions. The width of the rectangular channel in *X* direction was reduced to 0.76 mm while the width of that of Y direction was kept at 2.06 mm. Furthermore, the length of the reference medium increased approximately to twice the size of those printed samples used for the dimensional accuracy and repeatability. The dimensional accuracy of the 3DP specimen for the permeability measurements were well within the defined 2% limit of the overall thickness, which isolates the sources of variability due to geometrical factors.

Fig. 8: The side view of the porous medium in assumed *X* and *Y* directions: the dimensions of two pore structures (left) the rectangular channels with identical widths of 0.76 mm, (right) the rectangular channels with identical widths of 2.06 mm

The pressure gradient deduced from the pressure difference (ΔP) over the fluid viscosity (μ) is plotted as a function of the fluid velocity (v) in Fig.9. It is verified that the largest Reynolds number (Eq.2) of the flow encountered is lower than 1:

$$R_e^{max} = \frac{\rho v_{max} d}{\mu} = 7 \times 10^{-2} \qquad (2)$$

where ρ is the volume mass of the oil (875kg/m^3), v_{max} is the maximum fluid velocity encountered ($v_{max} \leq 1\times10^{-2}$ m /s), d is the largest characteristic length of the reference medium taken as the largest hydraulic diameter for the largest rectangular channel ($d \leq \frac{2\times height\times width}{height+width} = 2.29$ mm) and μ is the average fluid viscosity (286 mPa.s) measured before and after the permeability measurement at test temperature. The Reynolds number for the liquid composite moulding smaller than 10^{-1}, confirms the validity of Darcy's approach for these measurements [48]. The measurement of permeability components was carried out for this textile-like 3D printed sample. Fig.9 shows the typical measurement result. The pressure drop of the 3D printed porous medium varies linearly in accordance with the fluid velocity. Hence, the permeability can be determined as the inverse of the initial slope.

Fig. 9: Resistance of the 3D printed porous medium to the fluid flow versus the fluid velocity

The higher average permeability in y direction is consistent with the larger flow channels (2.06 mm). The comparison of the permeability components (Fig.9 and Fig.10) shows that the mean value of K_y is one order of magnitude greater than that of K_x which can be correlated to the channel size by Eq.3. Considering a rectangular

channel, having the width of b, and the height of a, with a slow, fully developed, steady-state flow along this channel, the meso-scale permeability of the channel is then calculated as [49]:

$$K_{meso-channel} = \frac{(a\times b)^3}{8(a+b)^2 A} \qquad (3)$$

where A is the cross-sectional area of the unit-cell. From Eq.3, K_y/K_x is about 9. Also, the dimensions of channels in the 3D printed sample are ten times larger than the flow channel sizes in real textile, leading to about 100 times greater permeability of the 3D printed sample than the common permeability values for the woven and non-crimp textiles. It should be noted that Eq.3 is valid for a long rectangular channel and it may significantly overestimate the permeability for complex, tortuous, and heterogeneous porous media.

3.2.2 Measurement of repeatability

Table Table 5 summarises statistical characterisations of K_x and K_y. As presented in Table 5 Table , the coefficient of variation (CV) of the permeability components are approximately 1.5%. This is significantly lower than the reported coefficient of variation of 15% for a certain standard three-dimensional woven fabric by Parnas and Salem [11], a coefficient of variation between 5% and 10% for fused PVC-coated material reported by Hoes and a coefficient of variation between 20% and 40% for typical textile preforms reported by benchmark II [8] and benchmark III [9,50]. The coefficient of variation levels presented in this paper are lower than the ones reported by Morren *et al.* [10] in the pioneering study of reference 3DP permeability specimens (CV of 3-6 % for permeability values and 1-6 % for anisotropy).

Table 5: Measured permeability components of the 3D printed porous medium at μ=286 mPa.s

As summarised in Table 5, the coefficient of variation of anisotropy ratio is relatively close to the coefficient of variation of the respective permeability components.

In order to take into account the uncertainty caused by the fluid viscosity, the permeability measurements for both directions were carried out at three different average fluid viscosity values (e.g. 77, 118, 277 mPa.s), measured before and after injection at test temperature. To reach the reported viscosity values, three types of the motor oil, namely, light, medium and heavy, were used. The densities of the light, medium and heavy oils were 850, 860, and 880 kg/m^3, correspondingly. Because of the precision of the reference medium and elimination of variability due to geometrical factors, the reference medium has good perspective to be used for studying effects of the physical parameters of the oil/test fluid (viscosity, shear thinning, density) on the apparent permeability.

Fig.10 shows that the ratio of pressure drop to flow rate ($\Delta P/Q$) for the 3D printed porous medium varies linearly in accordance with the fluid viscosity.

Fig. 10: Resistance of the 3D printed porous medium to the fluid flow versus the fluid viscosity

Table Table 6 summarises dependency of thef K_x and K_y values on the average fluid viscosity. It is observed that the change in viscosity led to CV of less than 2% in permeability components. These results show that the scatter on viscosity should not have an impact on the permeability measurement. More accurately accounting for viscosity can be addressed by measuring an in-line viscosity. The measurements of the in-line viscosity is a difficult task as the fluid's viscosity is affected by several factors such as temperature, air bubbles, shear rate, and so on. If temperature is a key contributing factor to the viscosity change and the other factors are kept relatively constant, then good control can be achieved by a real-time temperature reading of the fluid that is impregnating the porous medium.

Table 6: Measured permeability components of the 3D printed porous medium

Overall, our results, similar to the observation of Morren *et al.* [10], indicated that the CV of permeability obtained for the reference medium is significantly low (CV= less than 2%) when compared to other proposed reference porous media (CV=5-15%) and observed in the permeability benchmark II (CV=20%) [8] and benchmark III results (30-40%) [9].

In summary, our results confirmed that (i) the SLA technique can construct a robust textile-like reference medium with a suitable performance for the calibration of the permeability measurement set-ups, and (ii) the CV of permeability of printed porous medium by SLA in replicate measurements is less than 2%, which helps to eliminate the sources of variability inheret to real textils.

4. Conclusion

In this study, a printed textile-like porous medium that can be used as a reference sample for the calibration of permeability measurement equipment was produced with three different 3DP techniques: FDM, SLA, and MJF. Since the permeability is a geometrical parameter, the dimensional accuracy of the manufactured samples with the given techniques was evaluated. The measurements were carried out by LOM for the length and width of five different features,including solid tows, wall and pore geometries.. Finally, the best manufacturing method was selected to print a reference porous medium for the measurement of permeability.

The results of measurements were analysed by means of statistical analysis. For the textile-like porous specimen the following features of the field were observed:

(1) The standard deviation for the measurements of the specified features and the percentage of deviation from nominal size have the lowest values for the specimen printed by SLA technique.

(2) SLA technology is the best method which provided the high fidelity fine features on the surface and the precision was close to the designed dimensions.

(3) The sample printed by MJF technology has concave surface. This was more pronounced in the results of the wall features design of 9.2 mm × 2 mm. This problem was not observed in those specimens printed by FDM and SLA.

(4) The coefficient of variation of permeability components of 3D printed reference porous medium was less than 2%, confirming the elimination of the inherent source of variability in real textile; the value of the coefficient of variation lies within the tolerance of the mould dimentions prescribed by recommendations of the International Permeability Benchmarks.

Credit author statement

Masoud Bodaghi: Conceptualization, Methodology, Software, Resources, Validation, Formal analysis, Investigation, Writing-original Draft, Supervision, Review & Editing **D.Ban:** Validation, Formal analysis, Investigation, Resources **Mahmoud Mobin:** Formal analysis, Writing, Investigation **Chung Hae Park:** Review & Editing **Stepan V.Lomov:** Conceptualization, Methodology, Review & Editing **Mostafa Nikzad:** Conceptualization, Methodology, Software, Resources, Review & Editing, Visualization, Data Curation.

Acknowledgements

M.Bodaghi and CH.Park would like to acknowledge for the financial support from the French National Research Agency (ANR) for the "COMP3DRE" project. M.Bodaghi thankfully acknowledges Eng. Fernando Daniel Silva for the primary concept of the porous medium at INEGI. The work in Leuven was partially funded by KU Leuven Research Council (project PERMEA C24/16/021). SVL holds the Toray Chair for Composite Materials @ K Leuven, the support of which is acknowledged. Support of Eric Choi, Andrew Tarlinton and Colin Dingfelder from Swinburne AMDC and MPDE departments is greatly appreciated for 3D printing specimen.

References

[1] Bodaghi M, Lomov S V., Simacek P, Correia NC, Advani SG. On the variability of permeability induced by reinforcement distortions and dual scale flow in liquid composite moulding: A review. Compos Part A Appl Sci Manuf 2019;120:188–210. https://doi.org/10.1016/j.compositesa.2019.03.004.

[2] Bodaghi M, Vanaerschot A, Lomov S V, Correia NC. On the stochastic variations of intra-tow permeability induced by internal geometry variability in a 2 / 2 twill carbon fabric. Compos Part A 2017;101:444–58. https://doi.org/10.1016/j.compositesa.2017.07.008.

[3] Lomov S V., Huysmans G, Luo Y, Parnas RS, Prodromou A, Verpoest I, et al. Textile composites: Modelling strategies. Compos - Part A Appl Sci Manuf 2001;32:1379–94. https://doi.org/10.1016/S1359-835X(01)00038-0.

[4] Mehdikhani M, Gorbatikh L, Verpoest I, Lomov S V. Voids in fiber-reinforced polymer composites: a review on their formation, characteristics, and effects on mechanical performance. J Compos Mater 2018.

[5] Park CH, Lee W Il. Modeling void formation and unsaturated flow in liquid composite molding processes : a survey and review. Jounranl Reinf Plast Compos 2011;30:957–77. https://doi.org/10.1177/0731684411411338.

[6] Vanaerschot A, Cox BN, Lomov S V., Vandepitte D. Experimentally validated stochastic geometry description for textile composite reinforcements. Compos Sci Technol 2016;122:122–9. https://doi.org/10.1016/j.compscitech.2015.11.023.

[7] Arbter R, Beraud JM, Binetruy C, Bizet L, Bréard J, Comas-Cardona S, et al. Experimental determination of the permeability of textiles: A benchmark exercise. Compos Part A Appl Sci Manuf 2011;42:1157–68. https://doi.org/10.1016/j.compositesa.2011.04.021.

[8] Vernet N, Ruiz E, Advani S, Alms JB, Aubert M, Barburski M, et al. Experimental determination of the permeability of engineering textiles: Benchmark II. Compos Part A Appl Sci Manuf 2014;61:172–84. https://doi.org/10.1016/j.compositesa.2014.02.010.

[9] May D, Aktas A, Advani SG, Berg DC, Endruweit A, Fauster E, et al. In-plane permeability characterization of engineering textiles based on radial flow experiments: A benchmark exercise. Compos Part A Appl Sci Manuf 2019;121:100–14. https://doi.org/10.1016/j.compositesa.2019.03.006.

[10] Morren G, Bottiglieri M, Bossuyt S, Sol H, Lecompte D, Verleye B, et al. A reference specimen for permeability measurements of fibrous reinforcements for RTM. Compos Part A Appl Sci Manuf 2009;40:244–50.

[11] Parnas RS, Salem AJ. A comparison of the unidirectional and radial in-plane flow of fluids through woven composite reinforcements. Polym Compos 1993;14:383–94. https://doi.org/10.1002/pc.750140504.

[12] Parnas RS, Flynn KM, Dal-Favero ME. A permeability database for composites manufacturing. Polym Compos 1997;18:623–33.

[13] Lundström TS, Gebart BR, Sandlund E. In-plane permeability measurements on fiber reinforcements by the multi-cavity parallel flow technique. Polym Compos 1999;20:146–54. https://doi.org/10.1002/pc.10342.

[14] Roy T, Tan H, Pillai KM. A Method to estimate the accuracy of 1-D flow based permeability measuring devices. J Compos Mater 2007;41:2037–55. https://doi.org/10.1177/0021998307074109.

[15] Tan H, Pillai KM. A method to estimate the accuracy of radial flow—based permeability measuring devices. J Compos Mater 2009;43:2307–32.

[16] Sears NA, Seshadri DR, Dhavalikar PS, Cosgriff-Hernandez E. A review of three-dimensional printing in tissue engineering. Tissue Eng Part B Rev 2016;22:298–310.

[17] Kumar S, Kruth J-P. Composites by rapid prototyping technology. Mater Des 2010;31:850–6.

[18] Gu DD, Meiners W, Wissenbach K, Poprawe R. Laser additive manufacturing of metallic components: materials, processes and mechanisms. Int Mater Rev 2012;57:133–64.

[19] Calignano F, Manfredi D, Ambrosio EP, Biamino S, Lombardi M, Atzeni E, et al. Overview on additive manufacturing technologies. Proc IEEE 2017;105:593–612.

[20] Ngo TD, Kashani A, Imbalzano G, Nguyen KTQ, Hui D. Additive manufacturing (3D printing): A review of materials, methods, applications and challenges. Compos Part B Eng 2018;143:172–96.

[21] Bourell DL, Leu MC, Rosen DW. Roadmap for additive manufacturing: identifying the future of freeform processing. Univ Texas Austin, Austin, TX 2009:11–5.

[22] Steen WM, Mazumder J. Laser material processing. springer science & business media; 2010.

[23] Frazier WE. Metal additive manufacturing: a review. J Mater Eng Perform 2014;23:1917–28.

[24] Adamidis O, Alber S, Anastasopoulos I. Investigation into 3D printing of granular media. Phys Model Geotech 2018;1:113–8. https://doi.org/10.1201/9780429438660-9.

[25] Alms JB, Correia N, Advani SG, Ruiz E. Experimental Procedures to Run Longitudinal Injections to

Measure Unsaturated Permeability of LCM Reinforcements. FPCM Collab 2010.
[26] Masood SH, Rattanawong W, Iovenitti P. Part build orientations based on volumetric error in fused deposition modelling. Int J Adv Manuf Technol 2000;16:162–8.
[27] Wang T-M, Xi J-T, Jin Y. A model research for prototype warp deformation in the FDM process. Int J Adv Manuf Technol 2007;33:1087–96.
[28] Sood AK, Ohdar RK, Mahapatra SS. Experimental investigation and empirical modelling of FDM process for compressive strength improvement. J Adv Res 2012;3:81–90.
[29] Dixit NK, Srivastava R, Narain R. Dimensional accuracy improvement of part fabricated by low cost 3D open source printer for industrial application. 2016 10th Int. Conf. Intell. Syst. Control, IEEE; 2016, p. 1–6.
[30] Azhikannickal E, Uhrin A. Dimensional Stability of 3D Printed Parts: Effects of Process Parameters. Ohio J Sci 2019;119:9–16.
[31] Lee SH, Park WS, Cho HS, Zhang W, Leu M-C. A neural network approach to the modelling and analysis of stereolithography processes. Proc Inst Mech Eng Part B J Eng Manuf 2001;215:1719–33.
[32] Huang Y-M, Lan H-Y. Dynamic reverse compensation to increase the accuracy of the rapid prototyping system. J Mater Process Technol 2005;167:167–76.
[33] Dimitrov D, Van Wijck W, Schreve K, De Beer N. Investigating the achievable accuracy of three dimensional printing. Rapid Prototyp J 2006.
[34] Senthilkumaran K, Pandey PM, Rao PVM. Influence of building strategies on the accuracy of parts in selective laser sintering. Mater Des 2009;30:2946–54.
[35] Shi Y, Wang Y, Chen J, Huang S. Experimental investigation into the selective laser sintering of high-impact polystyrene. J Appl Polym Sci 2008;108:535–40. https://doi.org/10.1002/app.27686.
[36] Singh S, Sharma VS, Sachdeva A. Application of response surface methodology to analyze the effect of selective laser sintering parameters on dimensional accuracy. Prog Addit Manuf 2019;4:3–12.
[37] Islam MN, Boswell B, Pramanik A. An investigation of dimensional accuracy of parts produced by three-dimensional printing. Proc. World Congr. Eng. 2013, IAENG; 2013, p. 522–5.
[38] Cho U, Wood KL, Crawford RH. Novel empirical similarity method for the reliable product test with rapid prototypes. Proc. DETC, vol. 98, 1998, p. 1998.
[39] Cho U, Wood KL, Crawford RH. Online functional testing with rapid prototypes: a novel empirical similarity method. Rapid Prototyp J 1998.
[40] Mahn JP, Bayly P V. Impact testing of stereolithographic models to predict natural frequencies. J Sound Vib 1999;224:411–30.
[41] Fee C, Nawada S, Dimartino S. 3D printed porous media columns with fine control of column packing morphology. J Chromatogr A 2014;1333:18–24.
[42] Hoes K, Dinescu D, Sol H, Vanheule M, Parnas RS, Luo Y, et al. New set-up for measurement of permeability properties of fibrous reinforcements for RTM. Compos - Part A Appl Sci Manuf 2002;33:959–69. https://doi.org/10.1016/S1359-835X(02)00035-0.
[43] Belov EB, Lomov S V., Verpoest I, Peters T, Roose D, Parnas RS, et al. Modelling of permeability of textile reinforcements: Lattice Boltzmann method. Compos Sci Technol 2004;64:1069–80. https://doi.org/10.1016/j.compscitech.2003.09.015.
[44] Wang Q, Mazé B, Tafreshi HV, Pourdeyhimi B. A note on permeability simulation of multifilament woven fabrics. Chem Eng Sci 2006;61:8085–8. https://doi.org/10.1016/j.ces.2006.09.043.
[45] Nabovati A, Llewellin EW, Sousa ACM. Through-thickness permeability prediction of three-dimensional multifilament woven fabrics. Compos Part A Appl Sci Manuf 2010;41:453–63. https://doi.org/10.1016/j.compositesa.2009.11.011.
[46] Park CH. Chapter 15 - Numerical simulation of flow processes in composites manufacturing. Adv. Compos. Manuf. Process Des., Elsevier Ltd.; 2015, p. 317–78. https://doi.org/10.1016/B978-1-78242-307-2.00015-4.
[47] Saunders RA, Lekakou C, Bader MG. Compression and microstructure of fibre plain woven cloths in the processing of polymer composites. Compos Part A Appl Sci Manuf 1998;29:443–54. https://doi.org/10.1016/S1359-835X(97)00092-4.
[48] Karahan M, Lomov S V., Bogdanovich AE, Mungalov D, Verpoest I. Internal geometry evaluation of non-crimp 3D orthogonal woven carbon fabric composite. Compos Part A Appl Sci Manuf 2010;41:1301–11. https://doi.org/10.1016/j.compositesa.2010.05.014.
[49] Verleye B, Croce R, Griebel M, Klitz M, Lomov SV, Morren G, et al. Permeability of textile reinforcements: Simulation, influence of shear and validation. Compos Sci Technol 2008;68:2804–10. https://doi.org/10.1016/j.compscitech.2008.06.010.
[50] De Parseval Y, Pillai KM, Advani SG. A simple model for the variation of permeability due to partial saturation in dual scale porous media. Transp Porous Media 1997;27:243–64.
[51] Salvatori D, Caglar B, Teixidó H, Michaud V. Permeability and capillary effects in a channel-wise non-

crimp fabric. Compos Part A Appl Sci Manuf 2018;108:41–52. https://doi.org/10.1016/j.compositesa.2018.02.015.
[52] Hoes K, Dinescu D, Sol H, Parnas RS, Lomov S. Study of nesting induced scatter of permeability values in layered reinforcement fabrics. Compos Part A Appl Sci Manuf 2004;35:1407–18. https://doi.org/10.1016/j.compositesa.2004.05.004.

Figure captions

Fig. 1: The schematics of the dual porosity: (a) a 2/2twill woven carbon composite cross section, orthogonal to the warp (channels between tows forming inter-tow porosity), (b) Fibres inside a tow (channels between the fibres forming intra-tow porosity) the images with permission from [6]

Fig. 2: Integrated flow diagram for the selection of 3DP technique for manufacturing tangible textile-like porous medium

Fig. 3: The schematic of the textile-like porous medium: (a) A CAD geometry of the textile-like porous medium (top). (b) The dimension of the textile-like porous medium (below)

Fig. 4: Photographs indicating dimensions of the textile-like porous medium: five random locations used for measurement of the selected features.

Fig. 5: The flow front pattern during the impregnation process

Fig. 6: Average measured length (a) and width (b) and percentage of deviation from nominal (c) length and (d) width of wall features with different design ratio of length to width fabricated by different 3DP techniques

Fig. 7: Average measured length (a) and width (b) and percentage of deviation from nominal (c) length and (d) width of pore features with different design ratio of length to width fabricated by different 3DP techniques.

Fig. 8: The side view of the porous medium in assumed *X* and *Y* directions: the dimensions of two pore structures (left) the rectangular channels with identical widths of 0.76 mm, (right) the rectangular channels with identical widths of 2.06 mm

Fig. 9: Resistance of the 3D printed porous medium to the fluid flow versus the fluid velocity

Fig. 10: Resistance of the 3D printed porous medium to the fluid flow versus the fluid viscosity

Table Captions

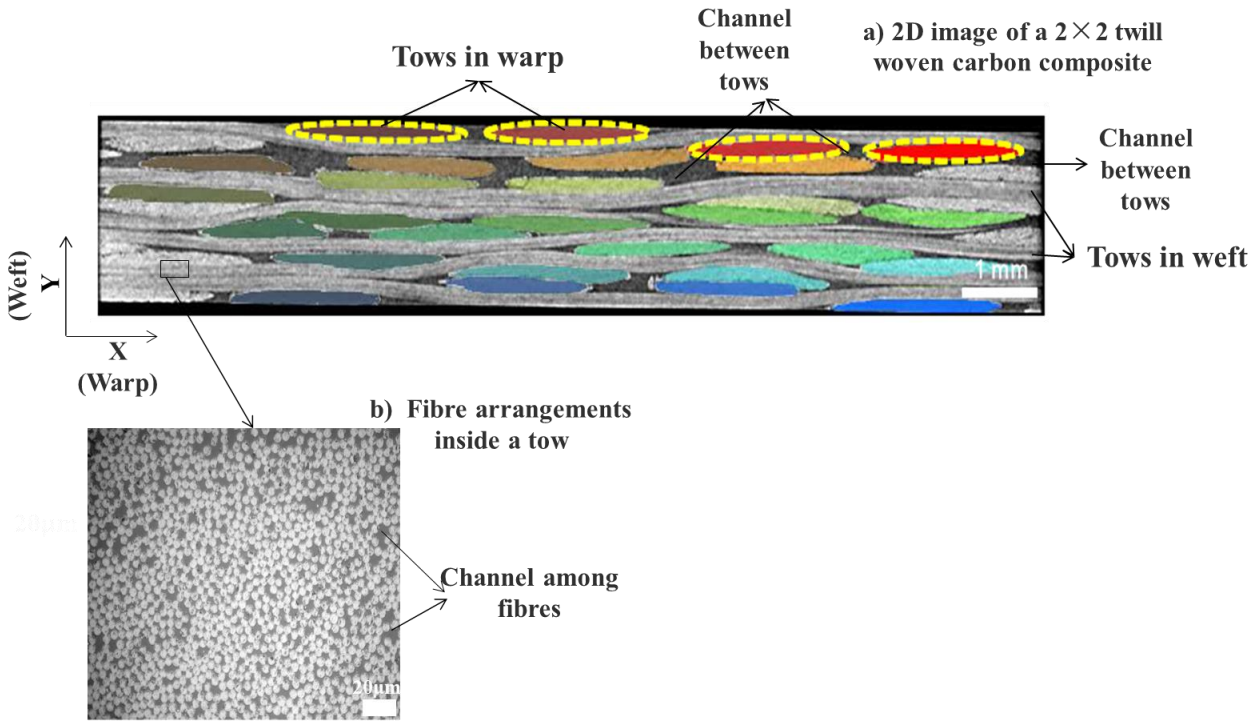

Fig. 1: The schematics of the dual porosity: (a) a 2/2twill woven carbon composite cross section, orthogonal to the warp (channels between tows forming inter-tow porosity), (b) Fibres inside a tow (channels between the fibres forming intra-tow porosity) the images with permission from [6].

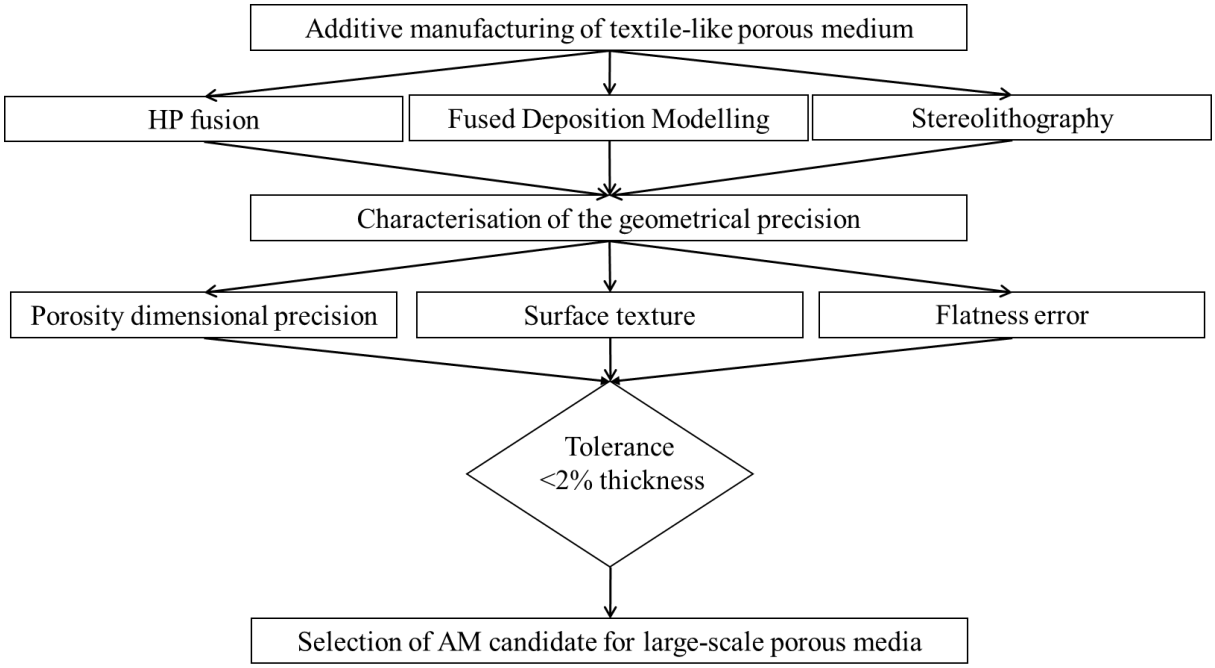

Fig. 2: Integrated flow diagram for the selection of 3DP technique for manufacturing tangible textile-like porous medium

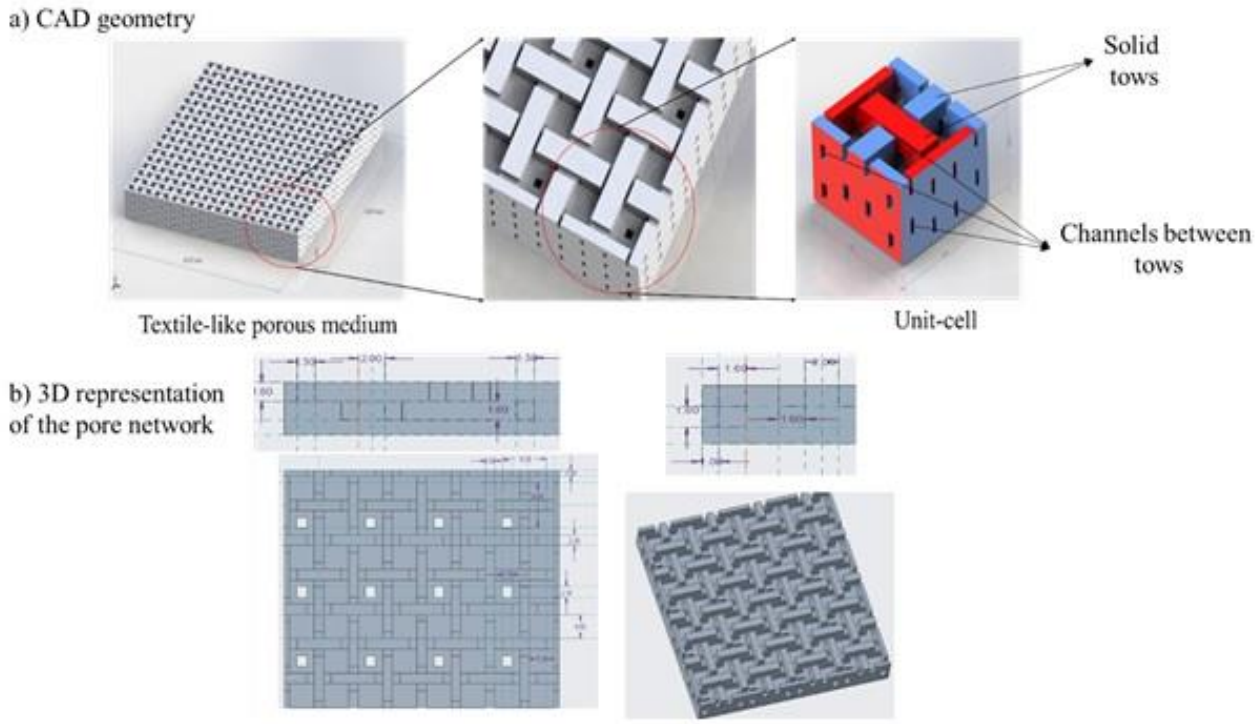

Fig. 3: The schematic of the textile-like porous medium: (a) A CAD geometry of the textile-like porous medium (top). (b) The dimension of the textile-like porous medium (below)

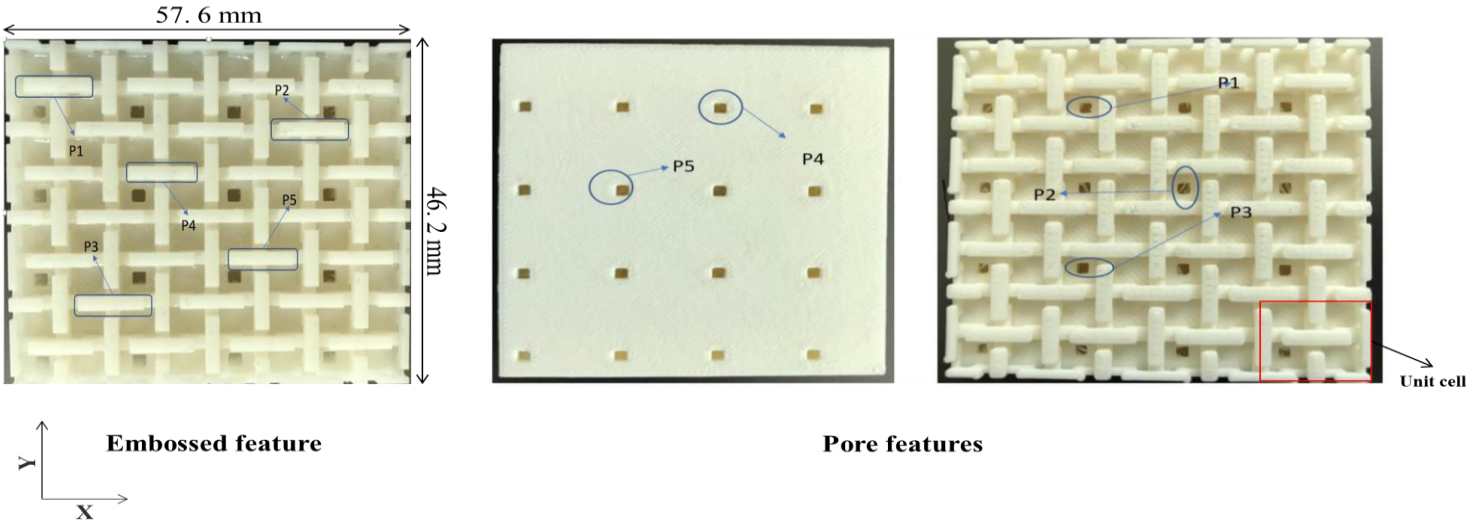

Fig. 4: Photographs indicating dimensions of the textile-like porous medium: five random locations used for measurement of the selected features.

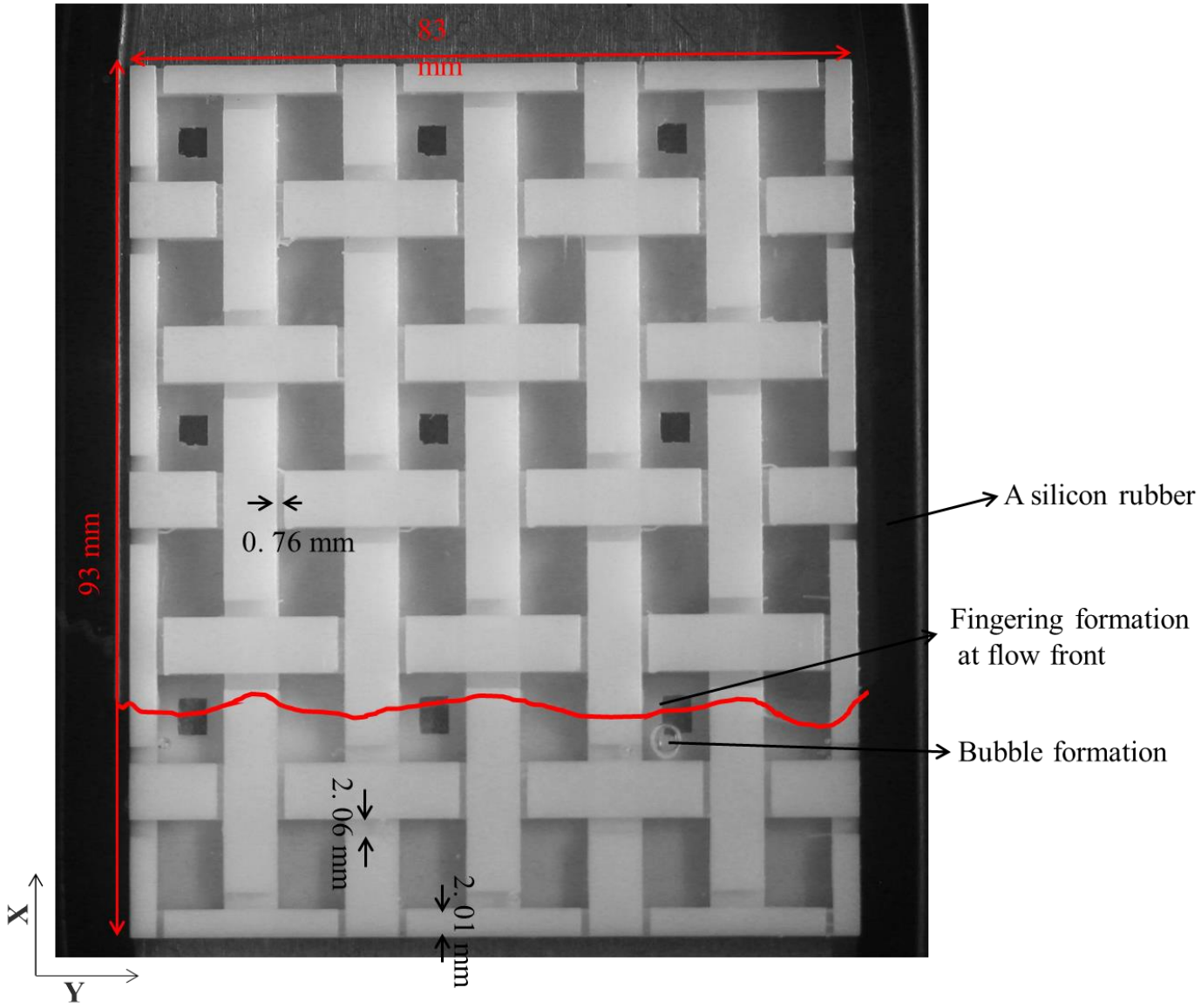

Fig.5: The flow front pattern during the impregnation process

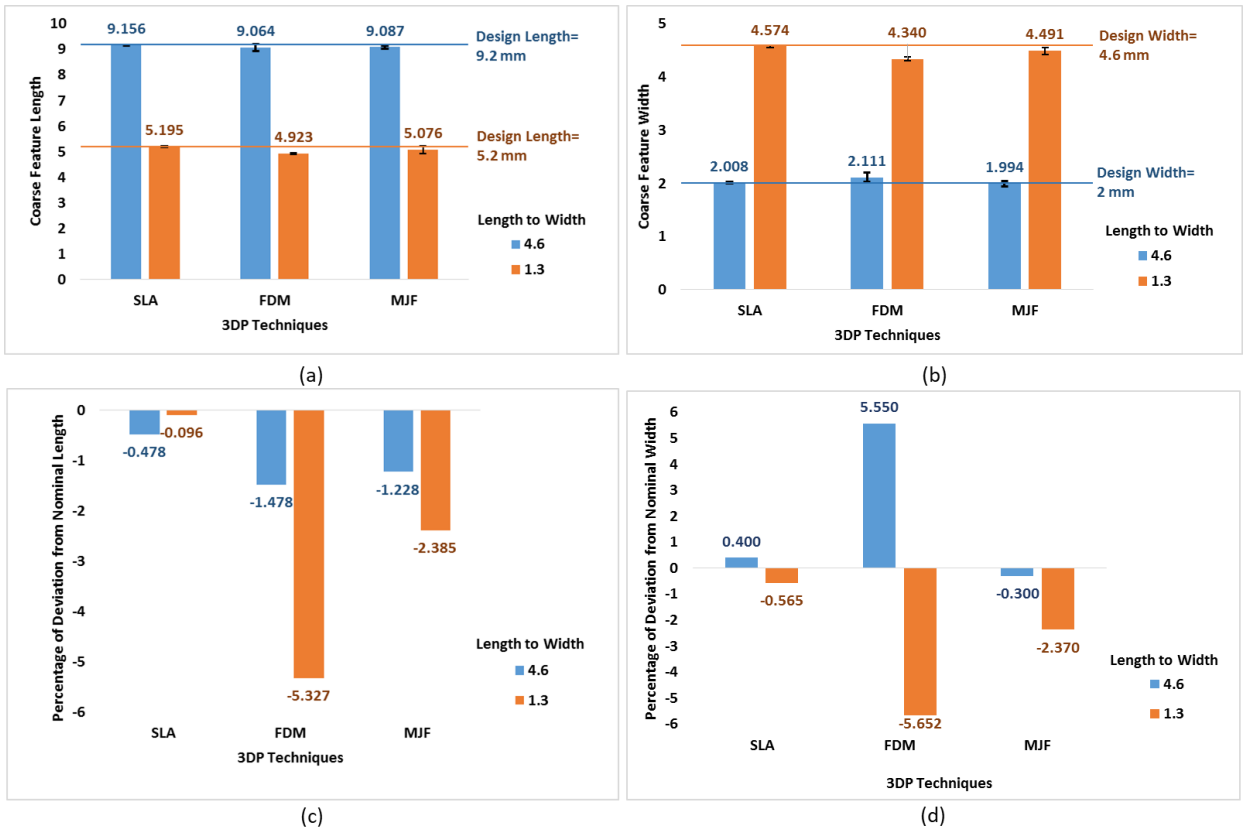

Fig. 6: Average measured length (a) and width (b) and percentage of deviation from nominal (c) length and (d) width of wall features with different design ratio of length to width fabricated by different 3DP techniques

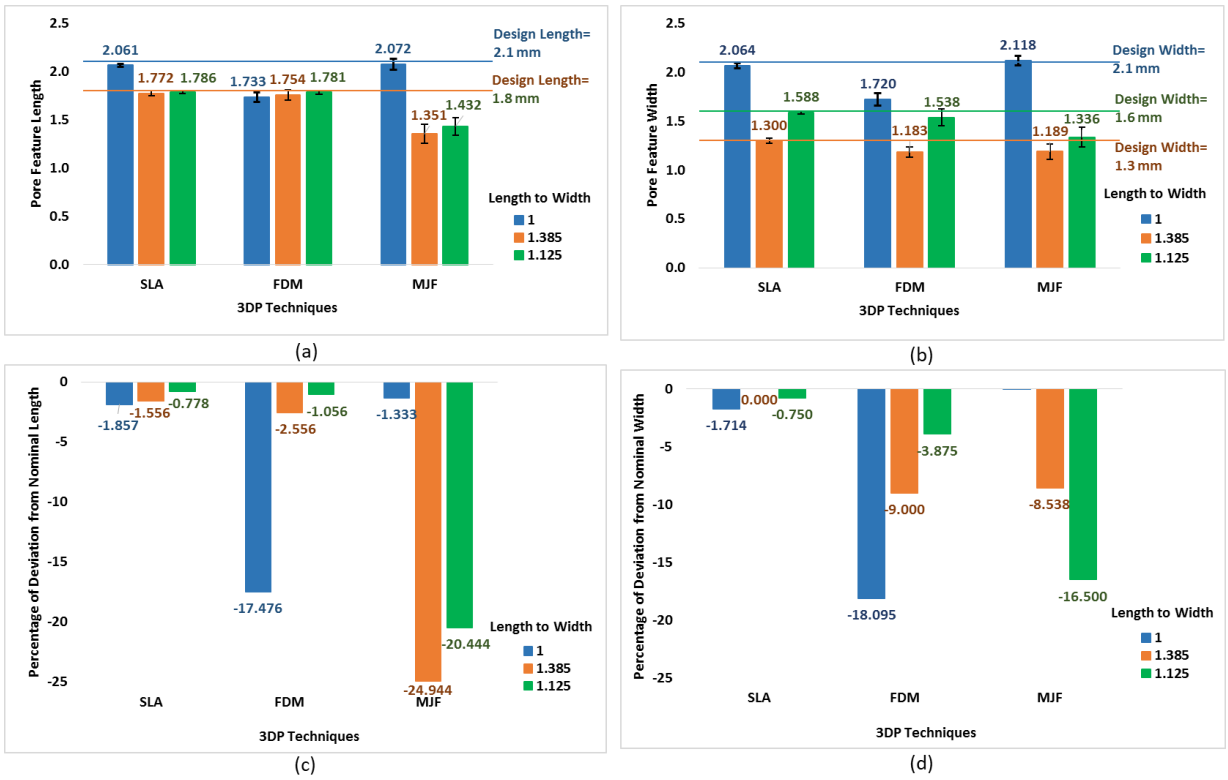

Fig. 7: Average measured length (a) and width (b) and percentage of deviation from nominal (c) length and (d) width of pore features with different design ratio of length to width fabricated by different 3DP techniques

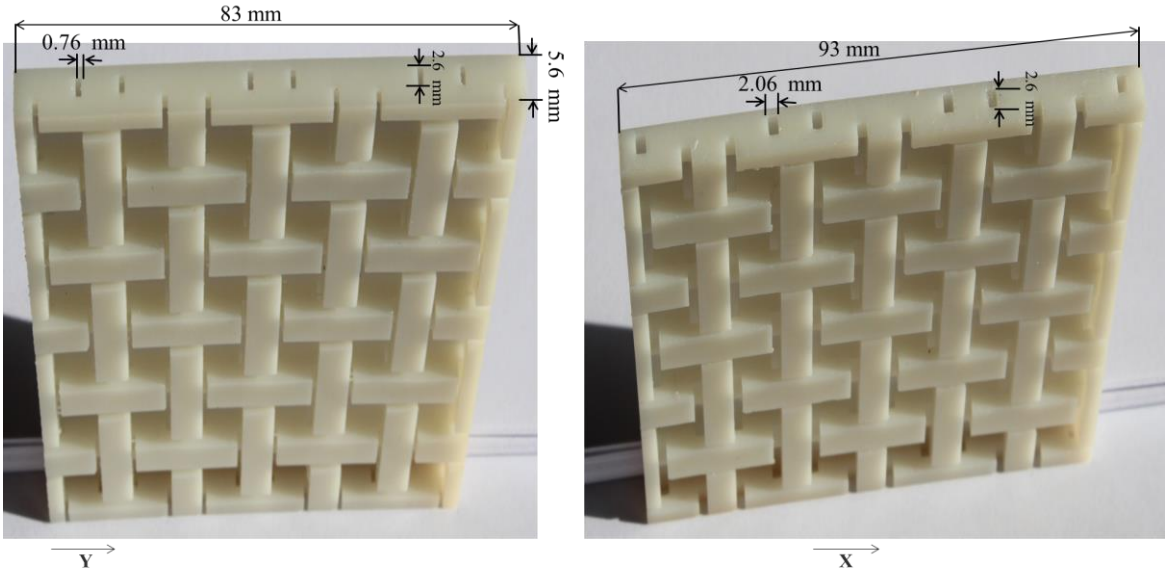

Fig. 8: The side view of the porous medium in assumed *X* and *Y* directions: the dimensions of two pore structures (left) the rectangular channels with identical widths of 0.76 mm, (right) the rectangular channels with identical widths of 2.06 mm

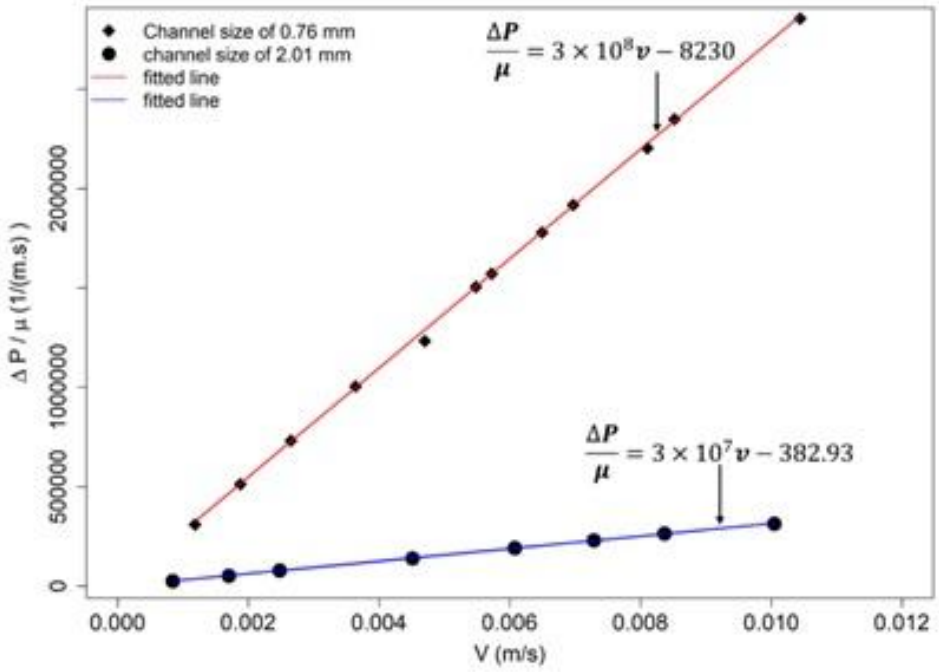

Fig. 9: Resistance of the 3D printed porous medium to the fluid flow versus the fluid velocity

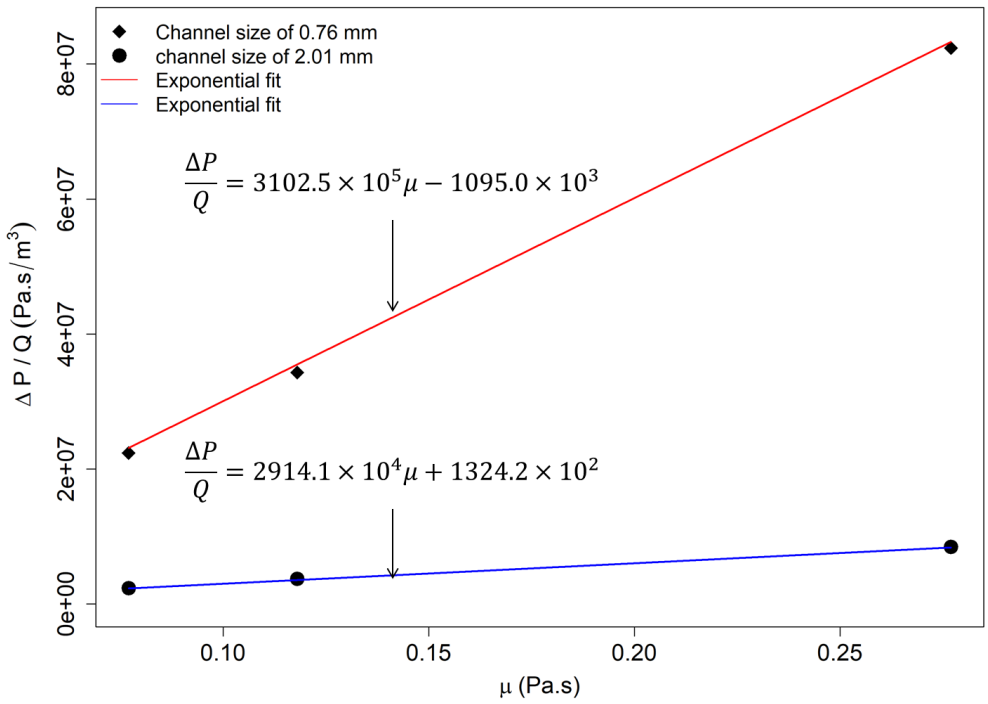

Fig. 10: Resistance of the 3D printed porous medium to the fluid flow versus the fluid viscosity

Table 1: The proposed criteria for a 3D printed reference medium for permeability measurements

Porous media characteristics: Solid, Rigid structure, Easy to clean and reused
Tolerance of the porosities: <2% of cavity height
Tolerance of convex features: <2% of cavity height
Roughness of surfaces: A good surface quality
Desired permeability variability: <5%

Table 2: Specifications of the used 3D printer machines

Tech.	Company	Apparatus	Material	Nominal XY Resolution	Nominal Z Resolution	Accuracy
SLA	3D Systems	ProJet 6000 HD	Thermoset Visijet SL Flux resin	DPI 4000 or 6.35 µm	50 um	0.025-0.05 mm per mm of part dimension
FDM	Zortax	M200	Thermoplastic Z- ABS filament	-	90 um	± 1.5 microns or ± 0.2 %
MJF	HP	3D Jet Fusion 4200	Thermoplastic Polyamide 12 powder	DPI 1200 or 21.17 µm	80 um	± 0.2 mm for parts up to 100 mm

Table 3: Measurement results of specified features for assessment of dimensional accuracy of AM techniques

Feature Type		Average and Standard Deviation* (μ±σ mm)		
Feature/ Location	Design Specification	SLA	FDM	MJF
Channel Wall/ XY Plane	Length= 9.2 mm	9.156±0.025	9.064±0.131	9.087±0.064
	Width= 2 mm	2.008±0.015	2.111±0.084	1.994±0.050
Channel Wall/ XY Plane	Length= 5.2 mm	5.195 ±0.016	4.923±0.029	5.076 ±0.152
	Width= 4.6 mm	4.574 ±0.027	4.340 ±0.039	4.491 ±0.063
Pores/ XY Plane	Length= 2.1 mm	2.061±0.018	1.733±0.047	2.072±0.054
	Width= 2.1 mm	2.064±0.025	1.720±0.063	2.118±0.047
Pores/ Z direction	Length= 1.8 mm	1.772±0.027	1.754±0.053	1.351±0.098
	Width= 1.3 mm	1.300±0.028	1.183±0.051	1.189±0.077
Pores/ Z direction	Length= 1.8 mm	1.786±0.017	1.781±0.019	1.432±0.091
	Width= 1.6 mm	1.588±0.013	1.538±0.083	1.336±0.099

*Calculated of 25 readings for each dimension.

Table 4: Results of single-factor ANOVA and multiple pairwise comparison tests

Feature Type		ANOVA	Tukey HSD Post Hoc Test		
Feature	Design Specification	P	P SLA-FDM	P SLA-MJF	P FDM-MJF
Channel Wall/ XY Plane	Length= 9.2 mm	7.593E-004	7.854E-004	1.400E-002	6.090E-001
		Sig.	Dif.	Dif.	Sim.
	Width= 2 mm	1.787E-010	5.405E-008	6.610E-001	6.338E-009
		Sig.	Dif.	Sim.	Dif.
Channel Wall/ XY Plane	Length= 5.2 mm	1.186E-015	5.101E-009	3.580E-001	2.226E-007
		Sig.	Dif.	Sim.	Dif.
	Width= 4.6 mm	9.680E-028	5.101E-009	3.900E-001	5.101E-009
		Sig.	Dif.	Sim.	Dif.
Pores/ XY Plane	Length= 2.1 mm	2.500E-043	5.101E-009	6.450E-001	5.101E-009
		Sig.	Dif.	Sim.	Dif.
	Width= 2.1 mm	2.385E-043	5.101E-009	4.046E-004	5.101E-009
		Sig.	Dif.	Dif.	Dif.
Pores/ Z direction	Length= 1.8 mm	1.071E-036	6.090E-001	5.101E-009	5.101E-009
		Sig.	Sim.	Dif.	Dif.
	Width= 1.3 mm	2.428E-011	5.629E-009	7.829E-009	9.220E-001
		Sig.	Dif.	Dif.	Sim.
Pores/ Z direction	Length= 1.8 mm	1.301E-037	9.400E-001	5.101E-009	5.101E-009
		Sig.	Sim.	Dif.	Dif.
	Width= 1.6 mm	7.394E-019	5.500E-002	5.101E-009	5.101E-009
		Sig.	Sim.	Dif.	Dif.

P= P-value, Sig.= Significant, Dif.= Difference, Sim.=Similarity

Table 5: Measured permeability components of the 3D printed porous medium at μ=286 mPa.s

Statistics	$K_x(\mu m)^2$ (flow channel of 0.76 mm)	$K_y(\mu m)^2$ (flow channel of 2.01 mm)	Anisotropy K_y/K_x
Number of observations	20	20	----
M= mean	3372	34824	10.32
S=Standard Deviation	79.5	584.7	0.2
CV(%)=S/M	1.76	1.68	1.93
Median	3346	34874	10.42
Minimum	3320	31498	9.48
Maximum	3421	35522	10.35

Table 6: Measured permeability components of the 3D printed porous medium

Statistics		$K_x(\mu m)^2$ (flow channel of 0.76 mm)	$K_y(\mu m)^2$ (flow channel of 2.01 mm)	Anisotropy K_y/K_x
Average viscosity (mPa.s)	77	3270	33500	10.24
	118	3390	33800	9.97
	277	3350	34600	10.32
M= mean		3276	33966	10.18
S=Standard Deviation		61.1	568.62	0.2
CV (%)=S/M		1.89	1.67	1.83